International Journal of Innovative Computing, Information and Control
Volume **12**, Number **5**, October **2016**

ICIC International ©2016 ISSN 1349-4198
pp. 1565–1579

BACKSTEPPING TERMINAL SLIDING MODE CONTROL OF DFIG FOR MAXIMAL WIND ENERGY CAPTURED

Zhongqiang Wu, Xinyi Wang and Xibo Zhao

College of Electric Engineering
Yanshan University
No. 438, Hebei Ave., Qinhuangdao 066004, P. R. China
mewzq@163.com

Received January 2016; revised July 2016

Abstract. *Doubly-Fed Induction Generator (DFIG) being taken as the research object, and the mathematical model based on the rotor flux orientation under two-phase synchronous rotating coordinate system being considered as two subsystems, the terminal sliding mode controllers based on backstepping are designed for them respectively and maximal wind energy captured is realized. The speed and flux observer of DFIG are designed by the nonsingular terminal sliding mode method, in which the high-order terminal sliding mode surface is used to suppress chattering effectively. The simulation results show that tracking without static error can be realized by the designed observer and controller and the characteristics such as quick response, good robustness and high precision have been got.*

Keywords: Terminal sliding mode, Maximal wind energy captured, Backstepping

1. **Introduction.** In recent years, the technology applications of doubly-fed wind power generation (DFIG) have become more and more widespread based on variable speed and constant frequency [1]. In order to realize decouple between active and reactive power [2], the vector control based on the stator flux orientation is usually used. Because of the complicated nonlinearity and strong couple of DFIG, it is difficult to get high accuracy control. In addition, most DFIGs have speed sensors, such as photoelectric encoder, and those devices increase the cost of the whole system [3]. The rotor speed observation of DFIG can reduce the number of devices and the cost of system, so it is becoming a hot research topic [4]. In [5], a nonlinear control scheme is proposed for DFIG based on passivity and adaptively reduced order observer. The Euler model of DFIG is established, and the system is decomposed into two interconnected feedback passive subsystems. An electrical subsystem and a mechanical subsystem, meanwhile, the passivity-based control can independently modulate the active and reactive power of stator, which improves the robustness of the system. However, it needs the parameters of motor accurately and is sensitive to the changes of load, which is not benefit to the stable operation of DFIG. In [6], combining with the characteristics of DFIG, a speed estimator based on stator flux is proposed by a sliding-mode model reference adaptive method, and the sensorless speed control of DFIG has been realized; meanwhile, the continuous saturation function is introduced to deal with the chattering problem of high frequency. However, it requires a higher system model and the design is more complex. In [7], a modified model reference adaptive observer is used to observe the angular speed of rotor and position of DFIG, and the strategy is suitable to the whole range of wind speed. However, at the beginning of the process, there is a large overshoot, which threatens the stable operation of DFIG. In [8], the vector control of DFIG without sensors is proposed based on a speed-adaptive

reduced-order observer, and the sensitivity analysis of parameter shows that the observer has robustness for the parameter variations of machine in the normal operation regions. However, for the designed observer there is a deviation between the estimated speed and the actual speed. In [9], the proportional relation of stator and rotor current is used to analyze the relation of rotor current and observed rotor position indirectly, and a vector control strategy of DFIG based on PQ power and observed rotor position is proposed. The control strategy overcomes the drawback that incorrect observation takes place in other speed observers when they run at the synchronous speed. The control strategy proposed has wider speed range, and the control performance achieved is similar as the method in which wind speed sensor is used. However, the method has limitations to sub-synchronous and super-synchronous state. In [10], the active disturbance rejection control is introduced in the rotor-current model of DFIG based on the air gap flux-oriented vector control theory. The simulation results show that, when the wind speed changes, the active disturbance rejection control can get smaller overshoot and faster response speed, compared with PID controller, which suppresses the voltage fluctuation of the grid effectively. However, in this method, there is a steady state error, so the steady-state accuracy is not high.

In this paper, considering the nonlinearity of wind power generation system and the problem of maximal wind energy captured, the terminal sliding mode controller based on backstepping is designed, and the maximal wind energy captured is realized. A terminal sliding mode observer is designed to estimate the speed of rotor and flux of DFIG. In the method, not only the speed measurement devices are eliminated, the cost of system, the affection of external interferences are reduced and chattering is suppressed, but also the steady state can be reached very quickly, and high accuracy control is got.

The rest of the paper is organized as follows. The mathematical model is given in Section 2. Section 3 describes the problem of maximum wind energy captured. The controller and observer are designed in Section 4 and Section 5. The performances of the proposed schemes are investigated in Section 6. Finally, Section 7 concludes the paper.

2. **The Mathematical Model of DFIG.** The stator winding of DFIG connects to the infinite power grid directly, so we can regard the voltage magnitude and frequency of the stator as constants. In this paper, the stator flux orientation is adopted, then $\psi_{sd} = \psi_1$, $\psi_{sq} = 0$, and the difference of phase angle between stator voltage and flux linkage is 90°, so $u_{sd} = 0$, $u_{sq} = U_s$, $\psi_1 = U_s/\omega_1$. At this time, the state equation of DFIG in the two-phase synchronous rotating coordinate system is,

$$\begin{cases} \dot{\psi}_1 = -\dfrac{R_s L_m}{L_s} i_{rd} - \dfrac{R_s}{L_s}\psi_1 \\ \dot{i}_{rd} = \dfrac{1}{\sigma L_r} u_{rd} - \dfrac{R_r}{\sigma L_r} i_{rd} + (\omega_1 - \omega_r) i_{rq} \\ \dot{i}_{rq} = \dfrac{1}{\sigma L_r} u_{rq} - \dfrac{L_m}{\sigma L_s L_r}(\omega_1 - \omega_r)\psi_1 - (\omega_1 - \omega_r) i_{rd} - \dfrac{R_r}{\sigma L_r} i_{rq} \\ \dfrac{J}{n_p}\dot{\omega}_r = -T_e + T_m - B_e \omega_r \end{cases} \tag{1}$$

The torque equation is,

$$T_e = \frac{3 n_p L_m}{2 L_s} \psi_1 i_{rq} \tag{2}$$

The power equation of gear box is,

$$T_M \omega_f = T_m \omega_r = T_m \omega_f n_f \tag{3}$$

where ψ_{sd}, ψ_{sq} are the flux linkages of stator; u_{sd}, u_{sq} are the voltages of stator; i_{rd}, i_{rq} are the currents of rotor; u_{rd}, u_{rq} are the voltages of rotor; the subscripts d, q represent the component of d, q axis respectively; R_s, R_r are the resistance of stator and rotor respectively; L_s, L_r are the inductance of stator and rotor respectively; L_m is mutual inductance; $\sigma = 1 - L_m^2/(L_s L_r)$ is leakage inductance; $T_r = L_r/R_r$ is the time constant of rotor; $T_s = L_s/R_s$ is the time constant of stator; $\tau = L_m^2/(\sigma L_s L_r)$; ω_1 is synchronous angular speed; ω_r is the rotor angular speed of DFIG; T_m is mechanical torque; T_e is the electromagnetic torque; T_M is the output mechanical torque of wind turbine; ω_f is the angular speed of wind turbine; B_e is the damping coefficient of generator; J is the rotational inertia; n_f is the transmission ratio; n_p shows the pole pairs of generator.

3. **The Maximal Wind Energy Captured.** DFIG system is made up of a wind turbine and gear box, which can get wind power by the blade of wind turbine. According to Betz theory [11],

$$\begin{cases} P_M = \dfrac{1}{2}\rho\pi C_p(\lambda,\varphi)R^2v^3 \\ T_M = \dfrac{P_M}{\omega_f} \end{cases} \tag{4}$$

where P_M is the wind power captured by turbine; ρ is the density of air; v is the actual wind speed; R is the radius of wind turbine; $\lambda = \omega_r R/v$ is the tip speed ratio; φ is the pitch angle of wind turbine; $C_p(\lambda,\varphi)$ is the capture coefficient of wind energy, which is the function of λ and φ,

$$C_p(\lambda,\varphi) = 0.5176\left(\frac{116}{\lambda_1} - 0.4\varphi - 5\right)e^{-\frac{21}{\lambda_1}} + 0.0068\lambda \tag{5}$$

where $\frac{1}{\lambda_1} = \frac{1}{\lambda+0.08\varphi} - \frac{0.035}{\varphi^3+1}$.

Let the pitch angle $\varphi = 0°$, the relationship between $C_p(\lambda,\varphi)$ and λ is shown in Figure 1.

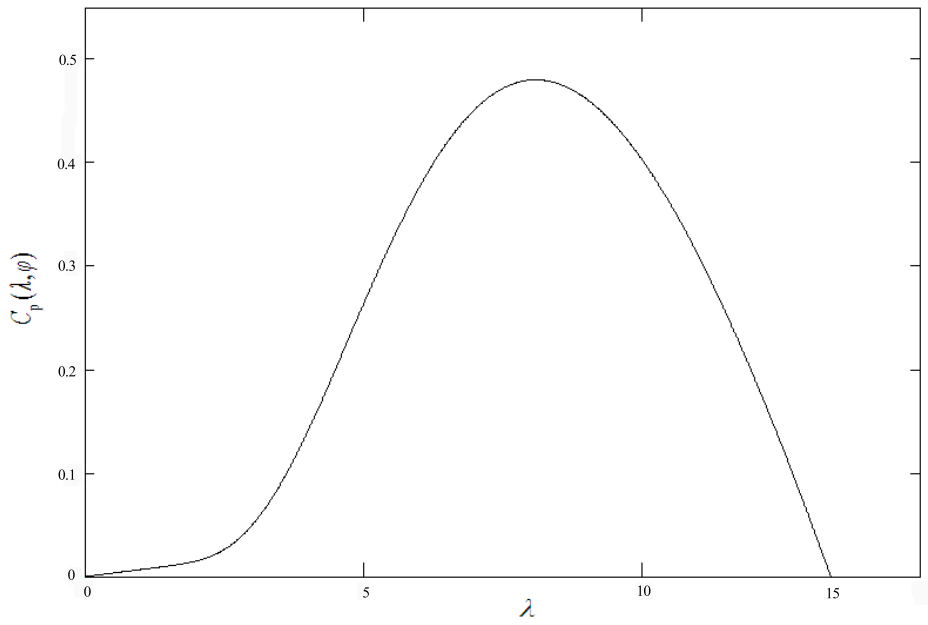

FIGURE 1. The curve of $C_p(\lambda,\varphi)$ and λ

As shown in Figure 1, when $\varphi = 0°$, the best tip speed ratio is $\lambda_{opt} = 8.1$, and the maximum wind energy captured coefficient is $C_{p.\max}(\lambda, \varphi) = 0.48$. According to the optimal tip speed ratio, the optimal angular speed of wind turbines can be got under different wind speeds $\omega_{fopt} = \lambda_{opt}\nu/R$. Then the optimal rotor angular speed of DFIG can be got, $\omega_{ropt} = n_f\omega_{fopt}$, which is regarded as a reference value of the rotor angular speed. When the maximum wind energy captured is realized, the relationship between the best power output and the angular speed of wind turbine [12] can be got by (4),

$$P_{Mopt} = h\omega_f^3 \tag{6}$$

where $h = \frac{1}{2}\pi\rho\left(R^5/\lambda_{opt}^3\right)C_{p.\max}$.

By (3)-(6) the relationship between the optimal input torque and rotor angular speed of DFIG can be got,

$$T_{mopt} = h\omega_r^2 \tag{7}$$

4. **The Design of Terminal Sliding Mode Controller Based on Backstepping.** Based on the mathematical model of DFIG, the objective of control is to design a controller $\boldsymbol{u} = [u_{rd} \;\; u_{rq}]^T$, so that the ψ_1 and ω_r track ψ_1^* and ω_{ropt} respectively. The design steps are that system (1) is divided into two subsystems, then terminal sliding mode controller is designed respectively.

Consider the subsystem 1 firstly,

$$\begin{cases} \dot{\psi}_1 = -\dfrac{R_sL_m}{L_s}i_{rd} - \dfrac{R_s}{L_s}\psi_1 \\ \dot{i}_{rd} = \dfrac{1}{\sigma L_r}u_{rd} - \dfrac{R_r}{\sigma L_r}i_{rd} + (\omega_1 - \omega_r)i_{rq} \end{cases} \tag{8}$$

Define the state tracking error of subsystem 1 as

$$\begin{cases} z_1 = \psi_1 - \psi_1^* \\ z_2 = i_{rd} - \alpha_1(\psi_1) \end{cases} \tag{9}$$

where $\alpha_1(\psi_1)$ is an intermediate control variable, and let $\alpha_1(\psi_1) = -\frac{L_s}{R_sL_m}\left(-c_1z_1 + \frac{R_s}{L_s}\psi_1\right)$, $c_1 > 0$.

Lyapunov function is selected as $V_{11} = \frac{1}{2}z_1^2$, according to (8) and (9),

$$\dot{V}_{11} = z_1\dot{z}_1 = z_1\dot{\psi}_1 = z_1\left(-\frac{R_sL_m}{L_s}i_{rd} - \frac{R_s}{L_s}\psi_1\right) = -\frac{R_sL_m}{L_s}z_1z_2 - c_1z_1^2 \tag{10}$$

As (10) shows that, if the designed control law makes z_2 converge, then $\dot{V}_{11} < 0$, which guarantees the subsystem composed of z_1 global stability. In order to make z_2 converge in a finite time, and improve the convergence rate and the steady-state tracking accuracy of system, the nonsingular terminal sliding mode surface is designed for z_2 subsystem as follows,

$$s_1 = z_2 + \gamma_1\dot{z}_2^{p/q} \tag{11}$$

where p, q are odd numbers, $1 < p/q < 2$, and $\gamma_1 > 0$.

The control law is designed as follows,

$$u_{rd} = u_1 + u_2 \tag{12}$$

$$u_1 = -\sigma L_r\left[-\frac{R_r}{\sigma L_r}i_{rd} + (\omega_1 - \omega_r)i_{rq} - \frac{c_1L_s}{R_sL_m}\dot{z}_1 - \frac{R_s}{L_s}\dot{\psi}_1\right] \tag{13}$$

$$u_2 = -\sigma L_r\int\left[\frac{1}{\gamma_1}\frac{q}{p}\dot{z}_2^{2-p/q} + \eta_1\mathrm{sgn}s_1\right]dt \tag{14}$$

where $\eta_1 > 0$ is a design parameter; therefore, the state of subsystem 1 can converge in a finite time.

According to the backstepping algorithm, the Lyapunov function is defined as follows.

$$V_{12} = \frac{1}{2}s_1^2$$

Take the derivative of V_{12} with respect to time.

$$\dot{V}_{12} = s_1\dot{s}_1 = s_1\gamma_1\frac{p}{q}\dot{z}_2^{p/q-1}\left(\ddot{z}_2 + \frac{1}{\gamma_1}\frac{q}{p}\dot{z}_2^{2-p/q}\right) \tag{15}$$

Because of

$$\dot{z}_2 = \dot{i}_{rd} - \alpha_1(\psi_1) = \sigma L_r u_{rd} - \frac{R_r}{\sigma L_r}i_{rd} + (\omega_1 - \omega_r)i_{rq} - \frac{c_1 L_s}{R_s L_m}\dot{z}_1 - \frac{R_s}{L_m}\dot{\psi}_1 \tag{16}$$

introduce (12) and (13) into (16).

$$\dot{z}_2 = \sigma L_r u_2$$

Take the derivative of $\dot{z}_2$ with respect to time once more,

$$\ddot{z}_2 = \sigma L_r \dot{u}_2$$

and then, introduce (14) into it.

$$\ddot{z}_2 = -\left(\frac{1}{\gamma_1}\frac{q}{p}\dot{z}_2^{2-p/q} + \eta_1 \mathrm{sgn}s_1\right) \tag{17}$$

At this time, introduce (17) into (15),

$$\dot{V}_{12} = -s_1\gamma_1\frac{p}{q}\dot{z}_2^{p/q-1}\eta_1\mathrm{sgn}s_1 = -\gamma_1\frac{p}{q}\dot{z}_2^{p/q-1}\eta_1|s_1|$$

where p, q are odd numbers, $1 < p/q < 2$, so $\dot{z}_2^{p/q-1} > 0$, and then $\dot{V}_{12} < 0$.

Consider subsystem 2 as follows.

$$\begin{cases} \dot{\omega}_r = -\dfrac{1.5n_p^2 L_m}{JL_s}\psi_1 i_{rq} + \dfrac{n_p}{J}K\omega_r^2 - \dfrac{B_e n_p}{J}\omega_r \\ \dot{i}_{rq} = \dfrac{1}{\sigma L_r}u_{rq} - \dfrac{L_m}{\sigma L_s L_r}(\omega_1 - \omega_r)\psi_1 - (\omega_1 - \omega_r)i_{rd} - \dfrac{R_r}{\sigma L_r}i_{rq} \end{cases} \tag{18}$$

And then, define the state tracking error of subsystem 2 as follows,

$$\begin{cases} z_3 = \omega_r - \omega_{ropt} \\ z_4 = i_{rq} - \alpha_2(\omega_r) \end{cases} \tag{19}$$

where $\alpha_2(\omega_r)$ is an intermediate control variable, and let $\alpha_2(\omega_r) = -\frac{JL_s}{1.5n_p^2 L_m\psi_1}\Big(-c_2 z_3 + \frac{B_e n_p}{J}\omega_r - \frac{n_p}{J}K\omega_r^2\Big)$; $c_2 > 0$.

Lyapunov function is selected as $V_{21} = \frac{1}{2}z_3^2$, according to (18) and (19)

$$\dot{V}_{21} = z_3\dot{z}_3 = z_3\dot{\omega}_r = -\frac{1.5n_p^2 L_m}{L_s J}\psi_1 z_3 z_4 - c_2 z_3^2 \tag{20}$$

As (20) shows that, if the designed control law makes z_4 convergence, then, $\dot{V}_{21} < 0$, which guarantees the subsystem composed of z_3 global stability. Similarly, the nonsingular terminal sliding mode surface for z_4 subsystem is designed as follows,

$$s_2 = z_4 + \gamma_2\dot{z}_4^{p/q} \tag{21}$$

where p, q are odd numbers, $1 < p/q < 2$, and $\gamma_2 > 0$.

The control law is designed as follows,

$$u_{rq} = u_3 + u_4 \tag{22}$$

$$\begin{aligned} u_3 = &-\sigma L_r \left[-\frac{L_m}{\sigma L_s L_r}(\omega_1 - \omega_r)\psi_1 - (\omega_1 - \omega_r) i_{rd} - \frac{R_r}{\sigma L_r} i_{rq} - \frac{c_2}{1.5 n_p^2 L_m \psi_1}\dot{z}_3 \right. \\ &\left. + \frac{L_s B_e}{1.5 n_p L_m \psi_1}\dot{\omega}_r - \frac{2 L_s K}{1.5 n_p L_m \psi_1}\omega_r \dot{\omega}_r \right] \end{aligned} \tag{23}$$

$$u_4 = -\sigma L_r \int \left[\frac{1}{\gamma_2}\frac{q}{p}\dot{z}_4^{2-p/q} + \eta_2 \mathrm{sgn} s_2 \right] dt \tag{24}$$

where $\eta_2 > 0$ is a design parameter; therefore, the state of subsystem 2 can converge in a finite time.

According to the backstepping algorithm, the Lyapunov function is defined as follows [13].

$$V_{22} = \frac{1}{2} s_2^2$$

Take the derivative of V_{22} with respect to time.

$$\dot{V}_{22} = s_2 \dot{s}_2 = s_2 \gamma_2 \frac{p}{q} \dot{z}_4^{p/q-1} \left(\ddot{z}_4 + \frac{1}{\gamma_2}\frac{q}{p}\dot{z}_4^{2-p/q} \right) \tag{25}$$

Because of

$$\begin{aligned} \dot{z}_4 &= \dot{i}_{rq} - \dot{\alpha}_2(\omega_r) \\ &= \sigma L_r u_{rq} - \frac{L_m}{\sigma L_s L_r}(\omega_1 - \omega_r)\psi_1 - (\omega_1 - \omega_r) i_{rd} - \frac{R_r}{\sigma L_r} i_{rq} + \frac{c_2 J L_s}{1.5 n_p^2 L_m \psi_1}\dot{z}_3 \\ &\quad - \frac{L_s B_e}{1.5 n_p L_m \psi_1}\dot{\omega}_r + \frac{2 L_s}{1.5 n_p L_m \psi_1} K \omega_r \dot{\omega}_r \end{aligned} \tag{26}$$

introduce (22) and (23) into (26).

$$\dot{z}_4 = \sigma L_r u_4$$

Take the derivative of $\dot{z}_4$ with respect to time once more,

$$\ddot{z}_4 = \sigma L_r \dot{u}_4$$

and then, introduce (24) into it.

$$\ddot{z}_4 = -\left(\frac{1}{\gamma_2}\frac{q}{p}\dot{z}_4^{2-p/q} + \eta_2 \mathrm{sgn} s_2 \right) \tag{27}$$

At this time, introduce (27) into (25)

$$\dot{V}_{22} = -s_2 \gamma_2 \frac{p}{q}\dot{z}_4^{p/q-1}\eta_2 \mathrm{sgn} s_2 = -\gamma_2 \frac{p}{q}\dot{z}_4^{p/q-1}\eta_2 |s_2| \tag{28}$$

where p, q are odd numbers, $1 < p/q < 2$, so $\dot{z}_4^{p/q-1} > 0$, and then $\dot{V}_{22} < 0$.

5. **The Design of Terminal Sliding Mode Observer for Speed and Flux.** By the current model in the DFIG model (1), the speed and flux observer based on the current of rotor are established as follows,

$$\begin{cases} \dot{\hat{i}}_{rd} = v_{rd} - \dfrac{R_r}{\sigma L_r}\hat{i}_{rd} + (\omega_1 - \omega_r)\hat{i}_{rq} \\ \dot{\hat{i}}_{rq} = v_{rq} - \dfrac{L_m}{\sigma L_s L_r}(\omega_1 - \omega_r)\psi_1 - (\omega_1 - \omega_r)\hat{i}_{rd} - \dfrac{R_r}{\sigma L_r}\hat{i}_{rq} \end{cases} \tag{29}$$

where $\hat{i}_{rd}$, $\hat{i}_{rq}$ are the estimated value of rotor current i_{rd}, i_{rq} respectively; v_{rd}, v_{rq} are the control signals of observer, which are instead of $\frac{1}{\sigma L_r}u_{rd}$, $\frac{1}{\sigma L_r}u_{rq}$ in the model (1) respectively. In (29), rotor speed ω_r and flux ψ_1 are the observed quantity ultimately; in fact, their observed values are calculated based on observed current values $\hat{i}_{rd}$, $\hat{i}_{rq}$. However, in the analysis and design of observer, they are usually seen as a known quantity for a moment, which does not affect the process of proof, and in the normal work of the observer, they should be taken place by the observed value $\hat{\omega}_r$, $\hat{\psi}_1$.

The observed error equation is,

$$\begin{cases} \dot{\bar{i}}_{rd} = v_{rd} - \dfrac{1}{\sigma L_r}u_{rd} - \dfrac{R_r}{\sigma L_r}\bar{i}_{rd} + (\omega_1 - \omega_r)\bar{i}_{rq} \\ \dot{\bar{i}}_{rq} = v_{rq} - \dfrac{1}{\sigma L_r}u_{rq} - \dfrac{R_r}{\sigma L_r}\bar{i}_{rq} - (\omega_1 - \omega_r)\bar{i}_{rd} \end{cases} \tag{30}$$

where $\bar{i}_{rd} = \hat{i}_{rd} - i_{rd}$, $\bar{i}_{rq} = \hat{i}_{rq} - i_{rq}$ are observed current error of rotor in the d, p axis. And error equation is written into vector form,

$$\dot{\bar{\boldsymbol{i}}} = \boldsymbol{v} - \frac{1}{\sigma L_r}\boldsymbol{u} + N\bar{\boldsymbol{i}} \tag{31}$$

where $\bar{\boldsymbol{i}} = [\bar{i}_{rd} \;\; \bar{i}_{rq}]^{\mathrm{T}}$, $\boldsymbol{v} = [v_{rd} \;\; v_{rq}]^{\mathrm{T}}$, $N = \begin{bmatrix} -\frac{R_r}{\sigma L_r} & \omega_1 - \omega_r \\ -(\omega_1 - \omega_r) & -\frac{R_r}{\sigma L_r} \end{bmatrix}$, $\boldsymbol{u} = [u_{rd} \;\; u_{rq}]^{\mathrm{T}}$.

The definition of nonsingular terminal sliding mode surface is,

$$\boldsymbol{s} = \bar{\boldsymbol{i}} + \boldsymbol{\gamma}\dot{\bar{\boldsymbol{i}}}^{p/q} \tag{32}$$

where $\boldsymbol{s} = [s_d \;\; s_q]^T$, $\boldsymbol{\gamma} = \mathrm{diag}\{\gamma_d \;\; \gamma_q\}$, $\gamma_d > 0$, $\gamma_q > 0$, p, q are odd numbers, $1 < p/q < 2$.

Nonsingular terminal sliding mode is used to realize second order sliding mode control, and chattering phenomenon is avoided. When $\boldsymbol{s}$ converges to zero, $\bar{\boldsymbol{i}}$ and $\dot{\bar{\boldsymbol{i}}}$ will converge to zero in a finite time. Then, the system keeps on the two-order sliding mode surface $\bar{\boldsymbol{i}} = \dot{\bar{\boldsymbol{i}}} = 0$.

The sliding surface (32) is selected for (31), and control law is designed as follows, then $\bar{\boldsymbol{i}}$ and $\dot{\bar{\boldsymbol{i}}}$ will converge to zero in a finite time:

$$\boldsymbol{v} = \boldsymbol{v}_{eq} + \boldsymbol{v}_n \tag{33}$$

$$\boldsymbol{v}_{eq} = \frac{1}{\sigma L_r}\boldsymbol{u} - N\bar{\boldsymbol{i}} \tag{34}$$

$$\boldsymbol{v}_n = -\int \frac{q}{p}\boldsymbol{\gamma}^{-1}\dot{\bar{\boldsymbol{i}}}^{2-\frac{p}{q}} + \beta \mathrm{sgn}\boldsymbol{s}dt \tag{35}$$

where $\beta > 0$.

Proof: The Lyapunov function is selected as $V_s = \frac{1}{2}\boldsymbol{s}^T\boldsymbol{s}$, so the derivative of V_s with respect to time is

$$\dot{\boldsymbol{V}}_s = \boldsymbol{s}^T\dot{\boldsymbol{s}} = (p/q)\boldsymbol{s}^{\mathrm{T}}\boldsymbol{\gamma}\mathrm{diag}\left\{\dot{\bar{\boldsymbol{i}}}^{p/q-1}\right\}\left[\ddot{\bar{\boldsymbol{i}}} + (q/p)\boldsymbol{\gamma}^{-1}\dot{\bar{\boldsymbol{i}}}^{2-p/q}\right] \tag{36}$$

Introduce (33) and (34) into (31).

$$\dot{\bar{\boldsymbol{i}}} = \boldsymbol{v}_n$$

Take the derivative of $\dot{\bar{\boldsymbol{i}}}$ with respect to time once more,

$$\ddot{\bar{\boldsymbol{i}}} = -(q/p)\boldsymbol{\gamma}^{-1}\dot{\bar{\boldsymbol{i}}}^{2-\frac{p}{q}} - \beta \mathrm{sgn}\boldsymbol{s}$$

then introduce (36) into it.

$$\dot{V}_s = (p/q)\boldsymbol{s}^{\mathrm{T}}\boldsymbol{\gamma}\mathrm{diag}\left\{\dot{\bar{\boldsymbol{i}}}^{p/q-1}\right\}[-\beta\mathrm{sgn}\boldsymbol{s}] = -(p/q)\boldsymbol{\gamma}\mathrm{diag}\left\{\dot{\bar{\boldsymbol{i}}}^{p/q-1}\right\}\beta\|\boldsymbol{s}\| < 0$$

The system converges to zero in a limited time.

When the system is in the steady state $\dot{\hat{i}}_{rd} = \dot{\hat{i}}_{rq} = 0$, according to $\hat{i}_{rd}$, $\hat{i}_{rq}$, (37) can be got by (29)

$$\begin{cases} \hat{\omega}_r = \left[v_{rd} - (R_r/\sigma L_r)\hat{i}_{rd} + \omega_1\hat{i}_{rq}\right] \Big/ \hat{i}_{rq} \\ \hat{\psi}_1 = \sigma L_s L_r \left[v_{rq} - (\omega_1 - \hat{\omega}_r)\hat{i}_{rd} - (R_r/\sigma L_r)\hat{i}_{rq}\right] \Big/ L_m(\omega_1 - \hat{\omega}_r) \end{cases} \tag{37}$$

Take the observed values into the controller,

$$\begin{aligned} u_{rd} = & -\sigma L_r \left[-\frac{R_r}{\sigma L_r} i_{rd} + (\omega_1 - \hat{\omega}_r)\, i_{rq} - \frac{c_1 L_s}{R_s L_m}\dot{z}_1 - \frac{R_s}{L_s}\dot{\hat{\psi}}_1\right] \\ & -\sigma L_r \int \left[\frac{1}{\gamma_1}\frac{q}{p}\dot{z}_2^{2-p/q} + \eta_1 \mathrm{sgn}s_1\right] dt \end{aligned}$$

$$\begin{aligned} u_{rq} = & -\sigma L_r \left[-\frac{L_m}{\sigma L_s L_r}(\omega_1 - \hat{\omega}_r)\,\hat{\psi}_1 - (\omega_1 - \hat{\omega}_r)\, i_{rd} - \frac{R_r}{\sigma L_r} i_{rq} - \frac{c_2}{1.5 n_p^2 L_m \hat{\psi}_1}\dot{z}_3 \right. \\ & \left. + \frac{L_s B_e}{1.5 n_p L_m \hat{\psi}_1}\dot{\hat{\omega}}_r - \frac{2L_s K}{1.5 n_p L_m \hat{\psi}_1}\hat{\omega}_r\dot{\hat{\omega}}_r\right] - \sigma L_r \int \left[\frac{1}{\gamma_2}\frac{q}{p}\dot{z}_4^{2-p/q} + \eta_2 \mathrm{sgn}s_2\right] dt \end{aligned}$$

The whole structure diagram of control system is as shown in Figure 2.

6. Simulation Research.

6.1. **Parameter setting.** The parameters of DFIG are set: rated power $P = 15$KW, rated voltage $U_N = 200$V. $R_s = 0.379\Omega$, $R_r = 0.314\Omega$, $L_s = 0.0438$H, $L_r = 0.0449$H, $L_m = 0.0427$H, $B_e = 1.25$, $\omega_1 = 105$rad/s, $J = 0.39\mathrm{kg/m}^2$, $n_p = 3$, $n_f = 8$, $\psi_1^* = -1$; The parameters of wind turbine are: $R = 4.3$, $\rho = 1.25\mathrm{kg/m}^3$; By repeated testing, the parameters of controller are set: $\gamma_1 = 0.1$, $\gamma_2 = 0.01$, $\eta_1 = 320$, $\eta_2 = 1000$, $c_1 = c_2 = 1$; The parameters of observer are set: $\gamma_d = 0.002$, $\gamma_q = 0.001$, $\beta = 15500$.

6.2. **The simulation results and analysis.** Case1: In order to test the effectiveness of the proposed scheme, the simulation is carried out under constant wind speed. The initial wind speed is set as 4m/s, at 6s, it changes into 7m/s, and when 12s, it changes into 10m/s. The curves of state variable are shown in Figures 3-5.

From Figure 3, it can be seen that adopting the terminal sliding mode method based on backstepping, not only the steady state is achieved in the limited time and chattering is avoided, but also tracking without static error is realized. The tracking error is less than 10^{-5}.

From Figure 4, at 0∼6s, the angular speed of rotor is at sub-synchronous speed, at 6s∼12s, it is close to the synchronous speed, and after 12s, it is at super-synchronous speed. When the angular speed of rotor is close to the synchronous speed, the rotor is

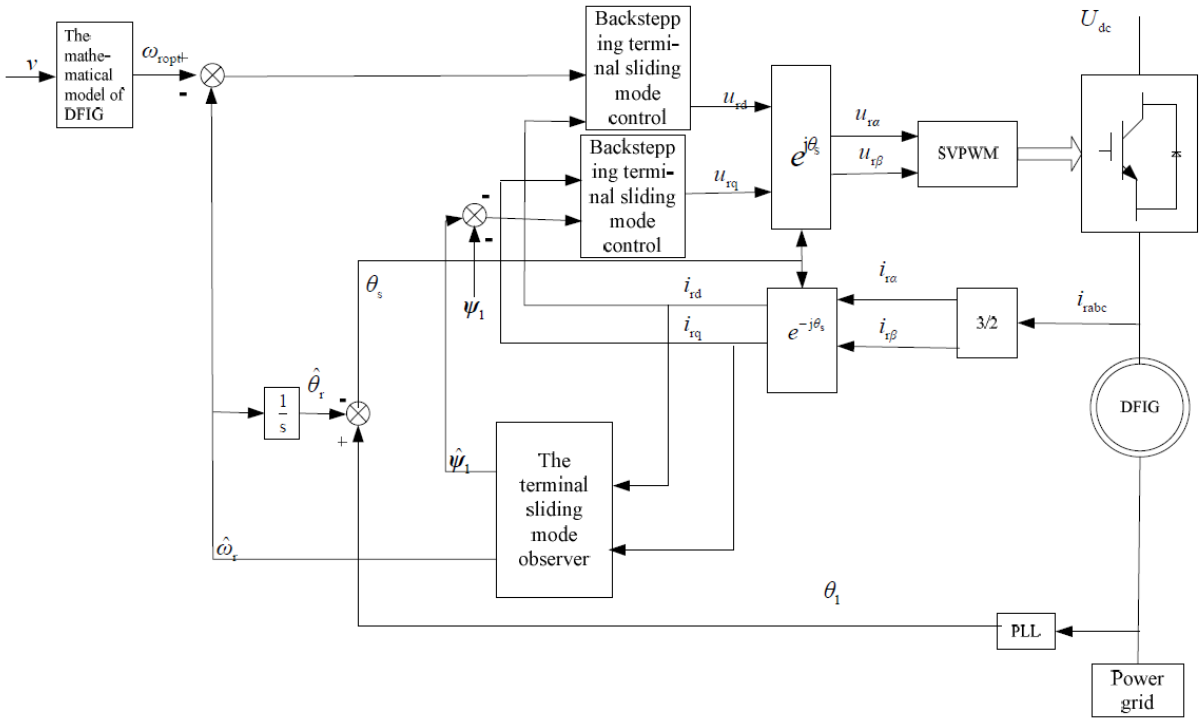

FIGURE 2. The principle diagram of DFIG control system

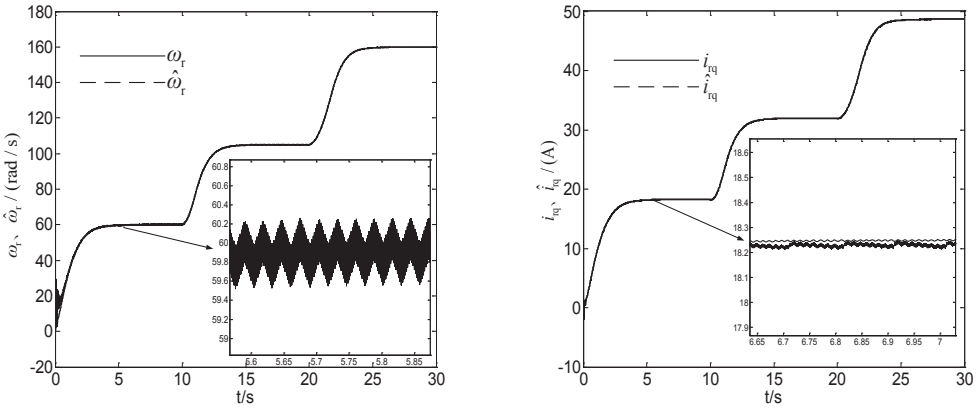

(a) The curve of ω_r and $\hat{\omega}_r$

(b) The curve of i_{rq} and $\hat{i}_{rq}$

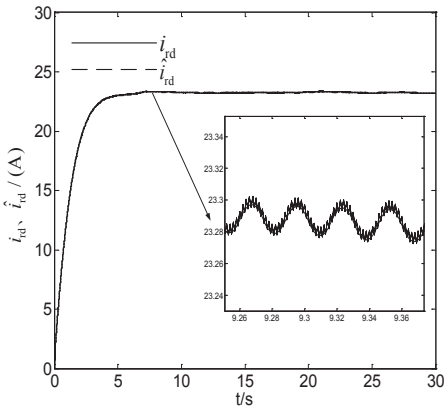

(c) The curve of i_{rd} and $\hat{i}_{rd}$

FIGURE 3. The curves of state variables and their estimations

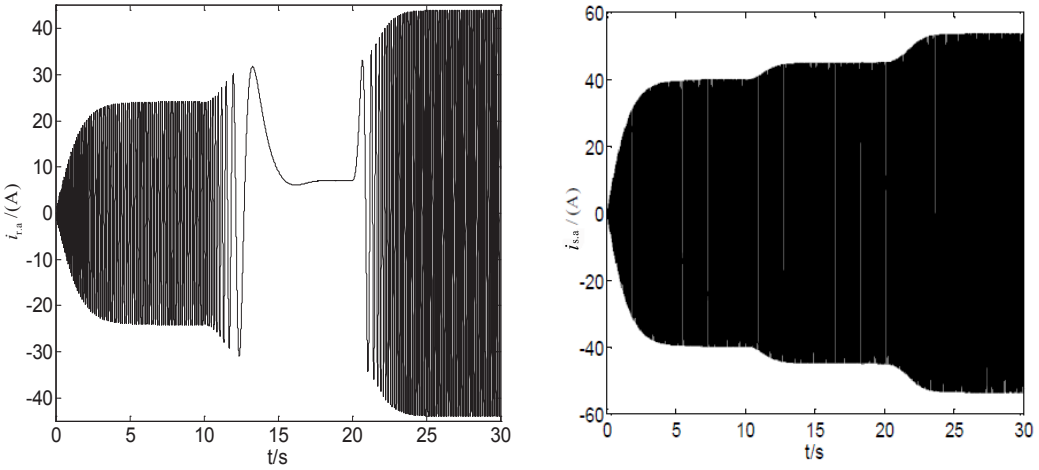

(a) The current curve of rotor in a phase (b) The current curve of stator in a phase

FIGURE 4. The current curve in a phase

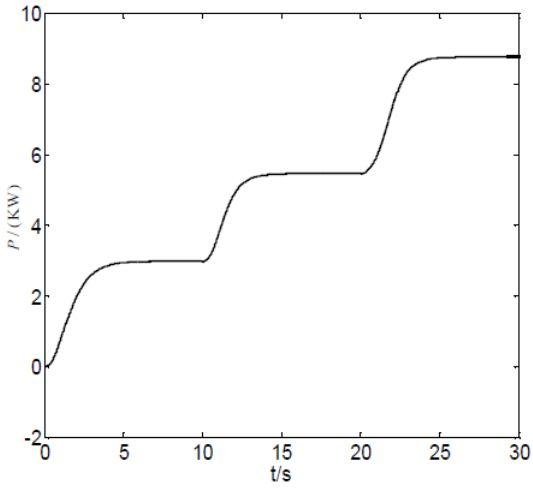

FIGURE 5. The active power curve of stator

in the state of DC excitation. At sub and super synchronous speed, the current of rotor turns to reverse while the frequency of the current of stator is always the same as that of the utility grid's, which conforms to the demand of variable speed and constant frequency. It also reflects the excellent performance of DFIG system as "flexible" connected to the utility grid in AC excitation state of VSCF (variable speed and constant frequency), which is inherent and irrelevant to the speed of generator.

According to the active power curve of stator in Figure 5, the analysis for the process of the maximum wind energy captured under the given wind speed is as follows. a) Firstly, the case of synchronous speed is analyzed. According to the operation principle of DFIG, at this time, all maximum wind power captured by wind turbine is changed into the output power of stator, and the power of rotor is only used for copper consumption. The maximum wind power captured by the wind turbine can be calculated by Formula (6) which is 6.12KW, and the output active power of the stator can be got from Figure 5 which is 5.45KW. The two values are similar, which conforms to the operation principle of DFIG, and the maximum wind energy captured is realized. b) In the sub-synchronous speed situation, the maximum wind power captured by wind turbine and the power of

the rotor are changed into the output power of the stator at this time. The maximum wind power captured by wind turbine can be calculated by Formula (6) which is 1.14KW, and the output active power of the stator can be got from Figure 5 which is 2.98KW. The output active power of the stator is larger than the maximum wind power captured by the wind turbine, which indicates that the rotor provides power for the stator. c) For the super-synchronous speed, the maximum wind power captured by the wind turbine is changed into the power of the rotor and the stator. The maximum wind power captured by the wind turbine can be calculated by Formula (6) which is 21.64KW, and the output active power of the stator can be got from Figure 5 which is 8.75KW. The maximum wind power captured by the wind turbine is larger than the output active power of the stator, which indicates that the wind turbine provides power for the rotor. Above all conform to the principles of operation of DFIG, and maximum wind energy captured is achieved.

Figure 6 shows the better curve of ω_r and $\hat{\omega}_r$ that adopted the disturbance rejection control method in [10], which is used to compare with the scheme in the paper.

A per unit speed is given in Figure 6. Compared with the speed in Figure 5, it can be seen that the fluctuation of transient process in [10] is obvious, and it also has a steady state error. In the paper, the overshoot of the transient process is very small, there is not static error, and high accuracy tracking is got.

Case2: In order to test the robustness of terminal sliding mode controller and observer, the simulation is carried out in the following two cases, and the error curves of the observed speed and the actual speed are obtained respectively: (1) When R_s, R_r are unchanged and the values of L_s, L_r, L_m are increased by 20%, the curve of $\Delta\omega_r$ and $\Delta\theta$ are shown in Figure 9 and Figure 10; (2) When L_s, L_r, L_m are unchanged and the values of R_s, R_r are increased by 20%, the curves of $\Delta\omega_r$ and $\Delta\theta$ are shown in Figure 11 and Figure 12. Figure 7 and Figure 8 are the curves of $\Delta\omega_r$ and $\Delta\theta$ in Case1 for comparison.

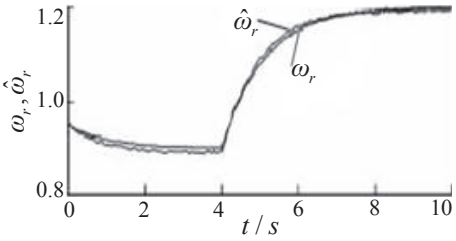

FIGURE 6. The curve of ω_r and $\hat{\omega}_r$ in [10]

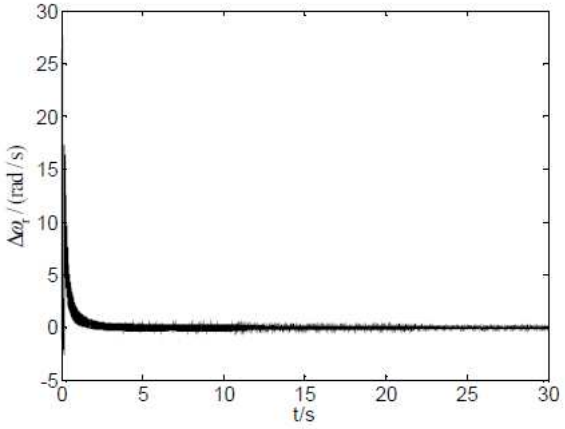

FIGURE 7. The curve of $\Delta\omega_r$ in Case1

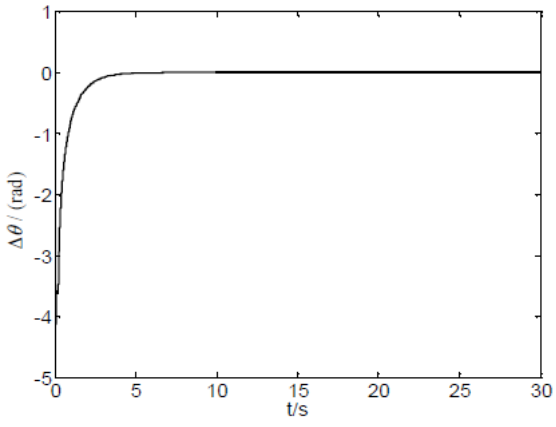

FIGURE 8. The curve of $\Delta\theta$ in Case1

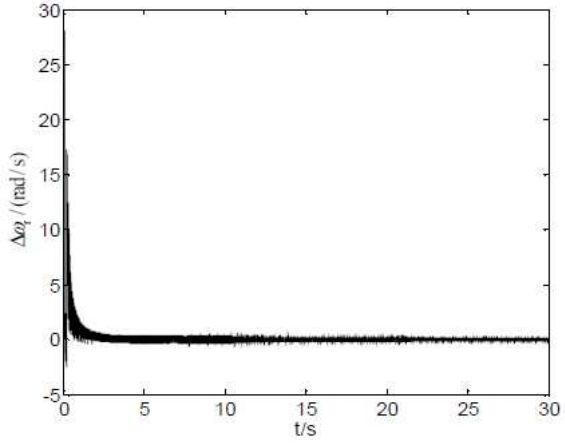

FIGURE 9. The curve of $\Delta\omega_r$ when L_s, L_r, L_m increase 20% respectively

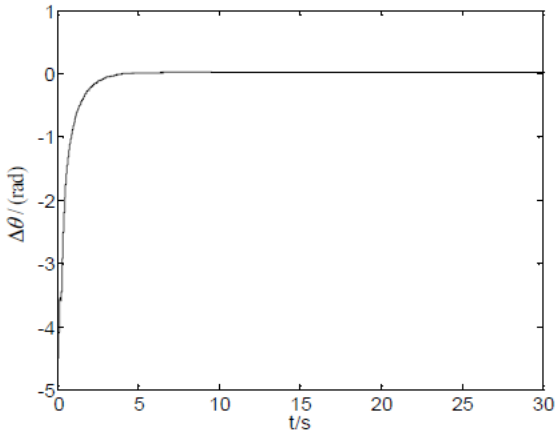

FIGURE 10. The curve of $\Delta\theta$ when L_s, L_r, L_m increase 20% respectively

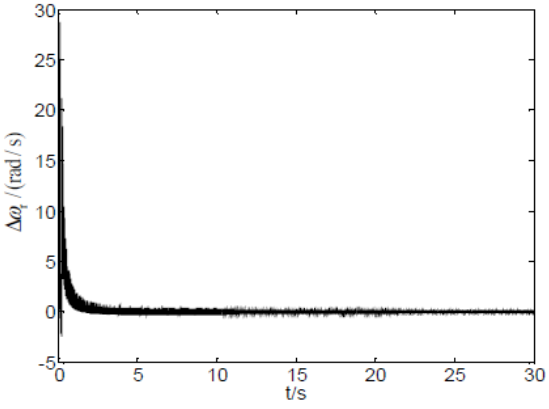

FIGURE 11. The curve of $\Delta\omega_r$ when R_s, R_r increase 20% respectively

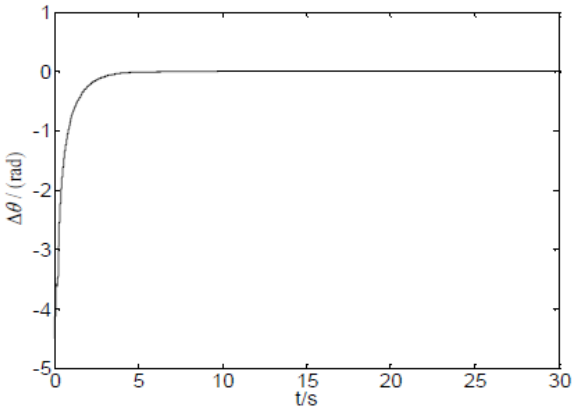

FIGURE 12. The curve of $\Delta\theta$ when R_s, R_r increase 20% respectively

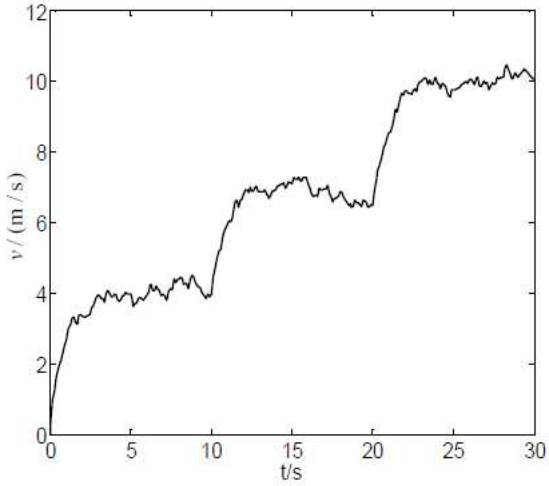

FIGURE 13. The curve of random wind speed

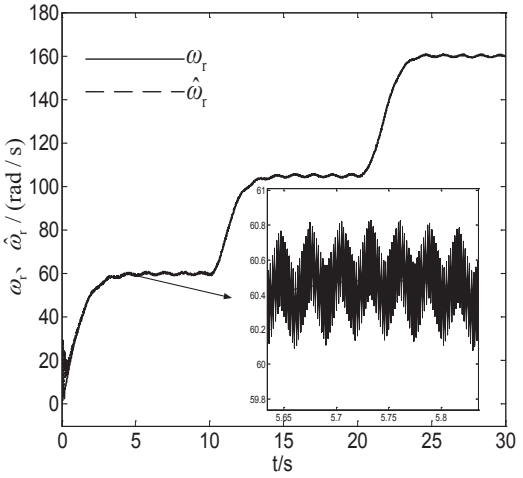

(a) The curve of ω_r and $\hat{\omega}_r$

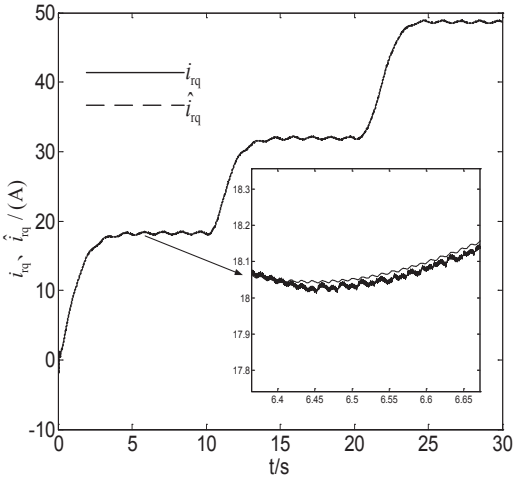

(b) The curve of i_{rq} and $\hat{i}_{rq}$

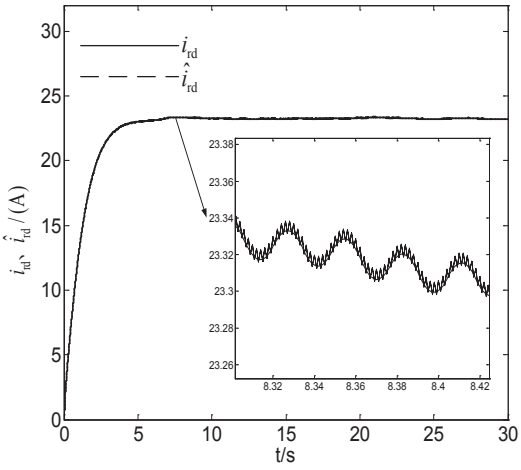

(c) The curve of i_{rd} and $\hat{i}_{rd}$

FIGURE 14. The curves of state variables and their estimations

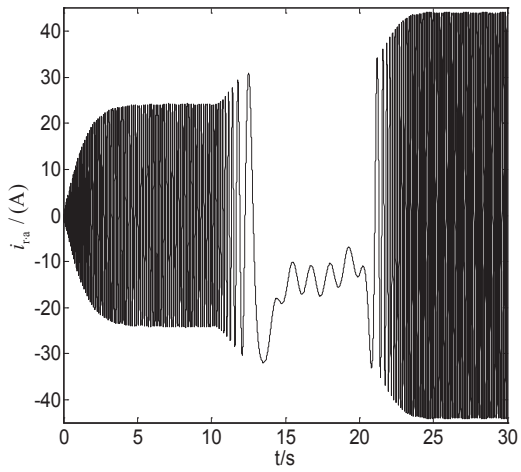

(a) The current curve of rotor in a phase

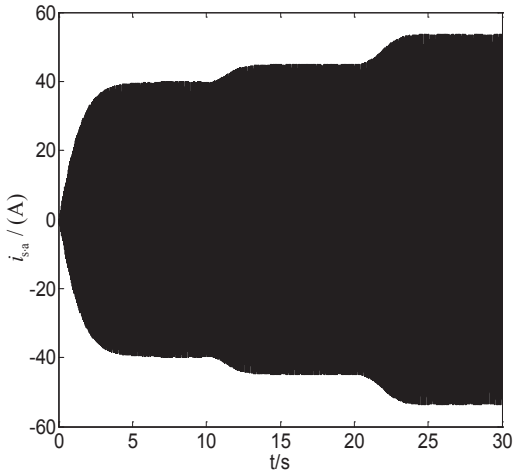

(b) The current curve of stator in a phase

FIGURE 15. The current curve in a phase

From Figures 7-12, it can be seen that when the resistance or inductance of generator has changed, the steady error between observed and actual angular speed is still within the permit limits, and the tracking error is less than 10^{-5}, similarly to angular. It shows the ability that in the sliding surface, the sliding mode controller and observer have robustness to the parameter changes of system.

Case3: Considering the practical application, the simulation under the random wind speed is carried out, the wind speed curve is shown in Figure 13, and the state variables of the system are shown in Figures 14 and 15.

From Figures 14 and 15, it can be seen that under the random wind speed, the maximum wind energy captured is still achieved by the designed observer and controller, which also meets the demand of VSCF.

7. **Conclusions.** In this paper, terminal sliding mode controller based on backstepping is designed, not only the robustness to external disturbance such as in common sliding mode is got, but also the convergence speed and the steady tracking accuracy are improved. In addition, the terminal sliding mode observer is used to observe the rotor angular speed of DFIG, so the speed sensors, such as photoelectric encoders have been saved and the cost of system has also been reduced. At the same time, the high-order terminal sliding mode technology is used to reduce chattering effectively, the control signal is smooth and low pass filtering and phase compensation component are avoided. The simulation results show that not only the maximal wind energy captured has been achieved, but also high control performance has been got. The proposed method is suitable for engineering application.

The future research directions are shown as follows: the research on nonlinear characteristic in other generators such as PMSG (Permanent magnet synchronous generator) and induction generator, and the designs of controller and observer based on nonlinear method; the engineering applications of those methods.

Acknowledgment. This work is supported by the Nature Science Foundation of Hebei Province (Project No. F2016203006). The authors also gratefully acknowledge the helpful comments and suggestions of the reviewers, which have improved the presentation.

REFERENCES

[1] M. Farshadnia and S. A. Taher, Current-based direct power control of a DFIG under unbalanced grid voltage, *International Journal of Electrical Power & Energy Systems*, vol.62, no.11, pp.571-582, 2014.

[2] A. Mohanty, M. Viswavandya, P. K. Ray et al., Stability analysis and reactive power compensation issue in a microgrid with a DFIG based WECS, *International Journal of Electrical Power & Energy Systems*, vol.62, no.11, pp.753-762, 2014.

[3] A. Susperregui, J. Jugo, I. Lizarraga and G. Tapia, Automated control of doubly fed induction generator integrating sensorless parameter estimation and grid synchronization, *IET Renewable Power Generation*, vol.8, no.1, pp.76-89, 2014.

[4] K. Belmokhtar et al., Novel fuzzy logic based sensorless maximum power point tracking strategy for wind turbine systems driven DFIG (doubly-fed induction generator), *Energy*, vol.76, pp.679-693, 2014.

[5] J. R. Wang, Y. R. Zhong and W. Z. Song, Doubly-fed induction generator control for wind power based on passivity and adaptively reduced order observer, *Proc. of the CSEE*, vol.31, no.33, pp.159-168, 2011.

[6] Q. L. Wang, Z. F. Wang, S. Y. Yang, Z. Xie and X. Zhang, Stator-flux-based sliding-mode MRAS speed estimation of doubly-fed wind power generator, *Journal of University of Science and Technology of China*, vol.44, no.7, pp.605-611, 2014.

[7] M. R. Esmaeeli, R. Kianinejad and M. Razzaz, Field oriented control of DFIG based on modified MRAS observer, *International Review on Modelling & Simulations*, pp.1-7, 2012.

[8] S. Yang and V. Ajjarapu, A speed-adaptive reduced-order observer for sensorless vector control of doubly fed induction generator-based variable-speed wind turbines, *IEEE Trans. Energy Conversion*, vol.25, no.3, pp.891-900, 2010.

[9] T. Liu, S. D. Huang, Q. L. Deng, G. F. Chen, Q. Y. Pu and D. T. Guo, Research on the control of doubly-fed induction wind power generator without speed sensor, *Control Engineering of China*, vol.20, no.5, pp.844-848, 2013.

[10] Z. Wei, X. Yu and J. Wu, Speed sensorless control of DFIG based on ADRC, *Electric Power Automation Equipment*, vol.31, no.1, pp.15-18, 2011.

[11] Z. Q. Wu, B. M. Ma and S. Y. Zhuang, Terminal sliding mode control of doubly-fed wind power generation system, *Electric Machines and Control*, vol.16, no.8, pp.94-100, 2012.

[12] Y. K. He, J. M. Hu and L. Xu, *Grid Connected Doubly Fed Induction Wind Generator Operation Control*, China Electric Power Press, Beijing, 2012.

[13] A. Levant, Higher-order sliding modes, differentiation and output-feedback control, *International Journal of Control*, vol.76, no.9, pp.924-941, 2003.